Review Articles

Artifacts and Pitfalls in Diffusion MRI

Denis Le Bihan, MD, PhD,* Cyril Poupon, PhD, Alexis Amadon, PhD, and Franck Lethimonnier, PhD

Although over the last 20 years diffusion MRI has become an established technique with a great impact on health care and neurosciences, like any other MRI technique it remains subject to artifacts and pitfalls. In addition to common MRI artifacts, there are specific problems that one may encounter when using MRI scanner gradient hardware for diffusion MRI, especially in terms of eddy currents and sensitivity to motion. In this article we review those artifacts and pitfalls on a qualitative basis, and introduce possible strategies that have been developed to mitigate or overcome them.

Key Words: diffusion; artifacts; MRI physics; eddy currents; EPI
J. Magn. Reson. Imaging 2006;24:478–488.

THE TERM "MOLECULAR DIFFUSION" refers to the random translational motion of molecules (also called Brownian motion) that results from the thermal energy carried by these molecules—a physical process that was well characterized by Einstein (1). In a free medium, during a given time interval, molecular displacements obey a three-dimensional Gaussian distribution: molecules travel randomly in space over a distance that is statistically well described by a "diffusion coefficient" (D). This coefficient depends only on the size (mass) of the molecules, and the temperature and the nature (viscosity) of the medium. For example, in the case of "free" water molecules diffusing in water at 37°C, $D = 3 \times 10^{-9}$ m^2 second^{-1}, which translates to a diffusion distance of 17 μm during 50 msec. About 32% of the molecules have reached at least this distance, while only 5% of them have traveled over distances greater than 34 μm. Water is the most convenient molecular species to study with diffusion MRI, but some metabolites may also be studied.

In the brain, the water molecular displacements significantly differ from the true "Brownian motion" defined for free molecules because water molecules bounce, cross, and interact with many tissue components, such as cell membranes, fibers, and macromolecules. In the presence of those obstacles, the actual diffusion distance is reduced compared to free water, and the displacement distribution is no longer Gaussian. In other words, while over very short times diffusion reflects the local intrinsic viscosity, at longer diffusion times the effects of the obstacles become predominant. Although the observation of this displacement distribution is made on a statistical basis, it provides unique clues about the structural features and geometric organization of neural tissues on a microscopic scale, as well as changes in those features with physiological or pathological states, which makes diffusion MRI a very powerful method (see Ref. 2 for a review).

Potential clinical applications of water diffusion MRI were suggested during its early days (3), but the most successful application since the early 1990s has been brain ischemia (4,5). With its unmatched sensitivity to changes in cell size, diffusion MRI provides some patients with the opportunity to receive suitable treatment at the acute stage of cytotoxic edema when brain tissue might still be salvageable. On the other hand, diffusion is truly a three-dimensional process, and hence molecular mobility in tissues may not be the same in all directions. Diffusion anisotropy was observed at the end of the 1980s in brain white matter (WM) (6). Diffusion anisotropy in WM originates from its specific organization in bundles of more or less myelinated axonal fibers running in parallel; however, the exact mechanism is still not completely understood in detail. Diffusion is faster in the direction of the fibers than in the perpendicular direction. It was soon recognized that this feature could be exploited to map out the orientation in space of the WM tracts in the brain (7). With the introduction of the more-rigorous formalism of the diffusion tensor (DT), diffusion anisotropy effects could be fully extracted, characterized, and exploited, providing even more exquisite details on tissue microstructure (8,9). The most advanced application is certainly that of fiber tracking in the brain, which in combination with functional MRI (fMRI) opens a new window into the important issue of brain connectivity (2). DT MRI (DTI) has also appeared as a promising tool for monitoring brain maturation and development (10,11), and especially the myelination process, as well

Anatomical and Functional Neuroimaging Laboratory, Service Hospitalier Frédéric Joliot, Commissariat à l'Energie Atomique, Orsay, France.

*Address reprint requests to: D.L.B., SHFJ/CEA, 4 Place du General Leclerc, 91401 Orsay, France. E-mail: denis.lebihan@cea.fr

Received February 23, 2006; Accepted May 30, 2006

DOI 10.1002/jmri.20683
Published online 8 August 2006 in Wiley InterScience (www.interscience.wiley.com).

as changes in connectivity in relation to functional disorders, such as psychiatric illnesses.

However, like any other MRI technique, diffusion MRI remains subject to artifacts and pitfalls. In this article, artifacts that one may encounter using diffusion MRI are reviewed in relation to their cause. The artifacts are explained and described on a qualitative basis, and possible strategies that have been developed to mitigate or overcome them are introduced. An extensive list of references is provided for readers who are interested in more technical or quantitative details.

HOW DIFFUSION MR IMAGES ARE MADE

While early water diffusion measurements were made in biological tissues using nuclear MR (NMR) in the 1960s and 1970s, it was not until the mid 1980s that the basic principles of diffusion MRI were laid out and applied to local measurements of water diffusion in vivo in the whole human brain (12–14; see Ref. 15 for a review).

MR signals can be made sensitive to diffusion through the use of a pair of sharp magnetic field gradient pulses (16), the duration and the separation of which can be adjusted. In an otherwise homogeneous field, the first pulse magnetically "labels" hydrogen nuclei (or protons) carried by water molecules according to their spatial location, as, for a short time, the magnetic field slowly varies along one direction. The second pulse is introduced slightly later to rephase hypothetical motionless spins and to detect nuclei that have changed location during the time interval (or "diffusion time") between the two pulses. A change in location (along the gradient direction) of a diffusing water hydrogen nucleus results in a change of the magnetic field "seen" by this nucleus, and a phase shift that is proportional to the net displacement (Fig. 1).

Considering now a population comprising a very large number of diffusing water molecules, the distribution of phase shifts corresponding to all hydrogen nuclei will reflect the distribution of all the water molecular displacements in this population through the magnetic field, and thus the statistical diffusion process. This distribution of phase shifts results in a slight attenuation of the MRI signal compared to the signal that could be obtained from a hypothetical population of completely static molecules or molecules diffusing in a perfectly homogeneous field. This signal attenuation is precisely and quantitatively linked to the degree of magnetic field variation experienced by the molecules, and hence to the amplitude of the displacement distribution. Fast (slow) diffusion results in a large (small) distribution of phase shifts, and in a large (small) signal attenuation. Of course, the effect also depends on the intensity and arrangement in time of the magnetic field gradient pulses, as represented by the so-called "b-factor" (3,12). It is important to note that only the diffusional displacement component *along* the gradient direction is detected.

In practice, one can sensitize any MRI technique to diffusion by inserting the adequate magnetic field gradient pulses (17). By acquiring data with various gradient pulse amplitudes, one can obtain images with different degrees of diffusion sensitivity. Contrast in these images depends on diffusion, but also on other MRI parameters, such as the water relaxation times. Hence, these images are often numerically combined to determine, using a global diffusion model, an estimate of the diffusion coefficient in each image location. The resulting images are maps of the diffusion process and can be visualized using a quantitative scale.

One must keep in mind, however, that the overall signal observed in a "diffusion" MR image volume element (voxel), at a millimetric resolution, results from the integration, on a statistical basis, of all the microscopic displacement distributions of the water molecules present in this voxel. As a departure from earlier biological studies in which efforts were made to depict the true diffusion process (18–20), Le Bihan et al (3) suggested that the complex diffusion processes that occur in a biological tissue on a voxel scale should be portrayed by using the microscopic, free-diffusion physical model, and replacing the physical diffusion coefficient, D, with a global statistical parameter, the apparent diffusion coefficient (ADC). With most current MRI systems, especially those developed for human applications, the voxel size remains large (a few mm^3). The averaging, smoothing effect resulting from this scaling presumes some homogeneity in the voxel and makes it difficult to obtain a direct physical interpretation from the global parameter, unless some assumptions can be made. The ADC depends not only on the actual diffusion coefficients of the water molecular populations present in the voxel, but also on experimental, technical parameters, such as the voxel size and the diffusion time. The relationship between the ADC and specific tissue microscopic features is currently the object of intensive research and is beyond the scope of this review.

ARTIFACTS AND LIMITATIONS FROM THE GRADIENT SYSTEM HARDWARE

The most specific artifacts result from the use of the strong gradient pulses that are necessary to encode the microscopic, diffusion-related molecular displacements.

First, the hardware used to generate these strong gradient pulses may cause problems. Since the minimum length of the molecular diffusion paths that are detectable with gradient-pulsed MRI is primarily determined by the intensity and duration of the gradient pulses (the b-factor), there is a need for hardware that is capable of providing stable gradients of the utmost intensity (21). This requirement may be extremely challenging when considering whole-body instruments designed for clinical studies. Therefore, the lack of gradient power is usually compensated for by the use of somewhat long gradient pulse widths, which makes diffusion measurements more difficult to treat and to interpret than those obtained with delta-function sharp pulses (15), since the diffusion time then becomes more difficult to characterize. There are partial solutions to this problem, such as using stimulated echoes to increase the effective diffusion time without penalizing the signal by T2 relaxation effects (22), using double spin-echo sequences (23), or, even better, by building

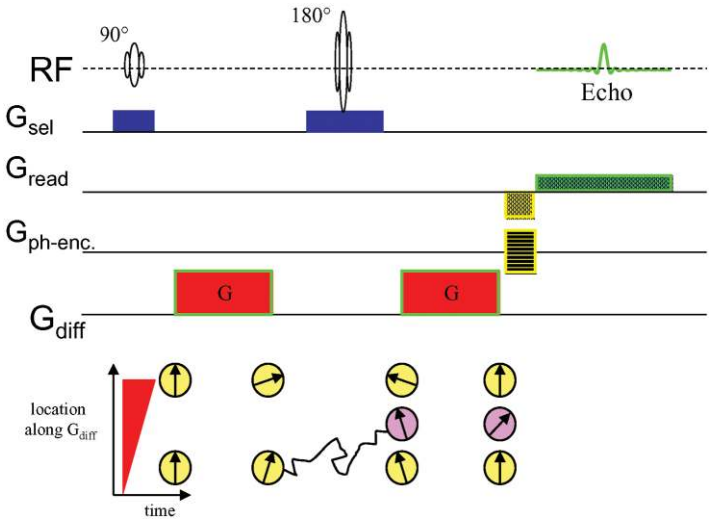

Figure 1. Spin-echo sequence sensitized to diffusion using a gradient pulse pair (G_{diff}). Spin phase-shift varies according to location along G_{diff}. Static spins are rephased by the 180° RF pulse and the second gradient pulse, while diffusing spins remain out of phase (G_{sl} = slice selection, G_{read} = readout, $G_{Ph\text{-}enc}$ = phase encoding). [Color figure can be viewed in the online issue, which is available at www.interscience.wiley.com.]

high-performance gradient coils (e.g., up to 40–100 mT/m and higher for animal systems). Safety should not be too much of a concern considering that slew rates will remain low because there is no need to switch the gradient coils very rapidly (which also limits eddy currents; see below).

Eddy Currents

In addition to nonlinearity (which leads to distortion (24)) and instability (which may arise when gradient amplifiers are driven hard for fast switching of large gradient intensities, and results in spiking from sparks in the gradient wires, and widely distributed ghost artifacts from random phase variations), the main source of problems with the gradient system comes from the eddy currents induced when strong gradient pulses are switched rapidly. When the diffusion gradient pulses are switched on and off, the time-varying magnetic field of the gradients results in current induction (eddy currents) in the various conducting surfaces of the rest of the MRI scanner. These, in turn, set up magnetic field gradients that may persist after the primary gradients are switched off (Fig. 2).

Eddy currents can originate in any conductive part of the MRI scanner (cryostat, RF coils, etc.) and scale up with the strength of the gradient pulses. In turn, the eddy currents generate magnetic field gradients that vectorially combine with the imaging gradient pulses such that the actual gradients experienced by spins in the imaged objects are not exactly the same as those that were programmed to produce and reconstruct the image. Accordingly, this error in the local gradients (which are not taken into account in the reconstruction software) produces geometric distortion in the final images. Three patterns can be observed in the diffusion-sensitized images: contraction or dilation of the image, and overall shift and shear (Fig. 3). Those distortions, which are easy to diagnose (e.g., by comparing diffusion-sensitized images with artifact-free anatomical images), become worse when the gradient pulses are stronger and may get very large.

Since quantitative diffusion images are calculated from MR images obtained with different degrees of diffusion sensitization (i.e., with different values for the b-factor), distortion will vary between them, and the resulting calculated diffusion images will be somewhat blurred and inaccurate. Another source of inaccuracy comes from the fact that the actual voxel size also varies slightly due to the mismatch between the actual local gradients and those assumed for image reconstruction. Since diffusion coefficients are calculated from at least two differently diffusion-sensitized images with slightly different voxel sizes, the calculated ADC may easily be over- or underestimated. Also, the b-factor actually "experienced" by water molecules differs slightly from the expected value, leading to over- or underestimation of the ADC. Since the b-factor scales with the square of the gradient strength, the effect may be far from negligible. One way to evidence this artifact is to use a "calibrated" phantom (e.g., water at a known and stable temperature, or a series of alkanes (25)), assuming, of

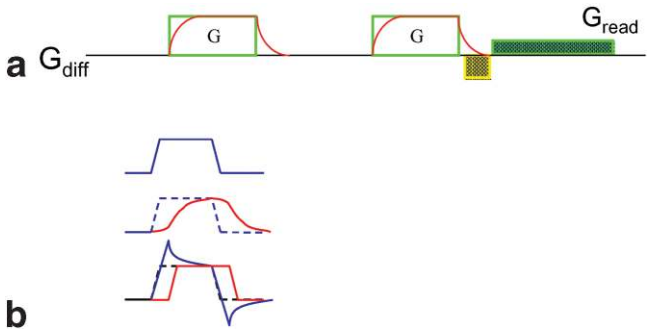

Figure 2. **a:** Effects of eddy currents on the actual shape of the diffusion gradient pulses (red). Eddy-current-induced gradients also interfere with the imaging gradients (here the readout gradient). **b:** Effect of preemphasis. Top: input of gradient amplifier (desired current output); middle: actual response of the gradient coil (red). **c:** Input with added preemphasis and the resulting response (red). [Color figure can be viewed in the online issue, which is available at www.interscience.wiley.com.]

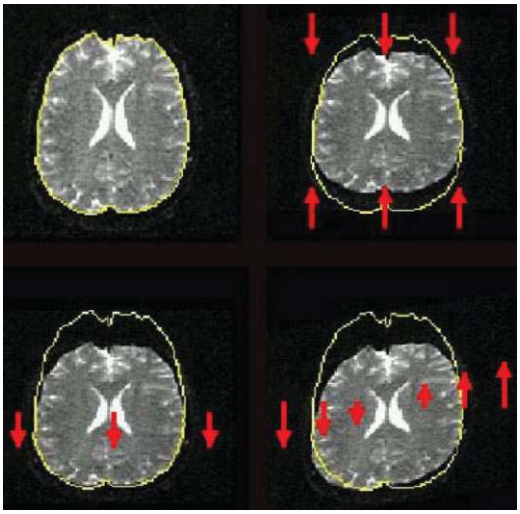

Figure 3. Three modes of distortion resulting from eddy currents: contraction (top right), shift (bottom left), and shear. [Color figure can be viewed in the online issue, which is available at www.interscience.wiley.com.]

course, that the gradient system itself has been correctly calibrated beforehand. Because eddy currents differ with the direction of the gradient pulses, the test should be repeated along the x, y, and z directions. In an isotropic phantom, the ADC must be the same in all directions. Any deviation points to eddy currents, a miscalibration, or nonlinearity of the gradient system (provided the b-factor is calculated properly, i.e., including diffusion and imaging gradient pulses, as well as their cross-terms (26,27)).

The use of a gradient coil of small dimensions that remains at a fair distance from the magnet core and can more easily generate large gradient amplitudes is certainly an attractive solution. However, the best cure for eddy currents is to use so-called "self-shielded" gradient coils, which are now standard in MRI systems. Additional wiring is used in such coils to decrease as much as possible the effects of the gradients outside the gradient coils (and thus in the cryostat) (28). However, eddy currents may still arise in other parts (e.g., the RF coils). The coils therefore must be designed to reduce the amount of large conductive surfaces using well known "tricks" (e.g., birdcage coils). Still, residual eddy currents will remain. A standard method consists of limiting the effects of eddy currents by purposely altering the shape of the currents sent to the gradient hardware. For instance, for a theoretical trapezoidal pulse, one can slightly increase the intensity of the currents on the upward and downward slopes of the pulse to compensate for the effects of eddy currents, which tend to oppose the currents. With proper calibration the actual gradients will have a trapezoidal shape. This operation, called "preemphasis" (29–31), should be done once and for all for a given MRI scanner; however, this is not easy because multiple corrections are necessary (for at least each of the x, y, and z axes, and also for several time constants, especially long-lasting ones; Fig. 2b).

Another concern with eddy currents is that any mismatch between the diffusion-sensitizing gradient pulses may cause artifactual signal losses due to an improper spin rephasing. If residual eddy current effects persist, other approaches can be combined (32–34). Finally, there is a possibility that the eddy currents will never be fully eliminated. Hope is not lost, since one may also use postprocessing software to correct for image distortion and ADC miscalculation (35,36). However, postprocessing should only be used in addition to other means of correcting eddy currents at the source.

MOTION ARTIFACTS

The second major source of artifacts, which is still related to the use of strong gradient pulses, is patient motion. While any MRI sequence is more or less prone to motion artifacts, diffusion MRI is exquisitely sensitive to motion. In the presence of the long and strong gradient pulses, microscopic, diffusion-driven water molecular displacements induce phase shifts. Since the motion is random and the molecules change directions many times during the presence of the gradient pulses (usually shorter than the TE), the distribution of phase shifts results in a loss of coherence and a signal amplitude attenuation that is used to calculate the ADC. At the same time, in the presence of tissue macroscopic motion (due to head motion, pulsating flow, etc.), spins experience large displacements that also result in large phase shifts (10 or 100 times larger than those induced by diffusion) as phase shifts increase with the strength of the gradient pulses. If all spins in a given voxel usually experience the same motion-driven displacement, there is no loss of coherence but only an overall phase shift of the signal, and there is no effect on the signal attenuation and the ADC. The problem arises when the sequence is repeated several times with different motion patterns. For instance, using a 2DFT spin-echo sequence with 256 lines, the image will be reconstructed from 256 echo signals acquired each TR interval. Each echo signal will have the same diffusion-induced echo attenuation because diffusion is a self-consistent process. However, there is no reason for the macroscopic motion to repeat itself identically each time. Hence, each echo will get a different overall phase shift depending on the amplitude and direction of the motion. The result of such a distribution of phase shifts over time and k-space is well known: the images will exhibit "ghosts" along the phase-encoding direction,

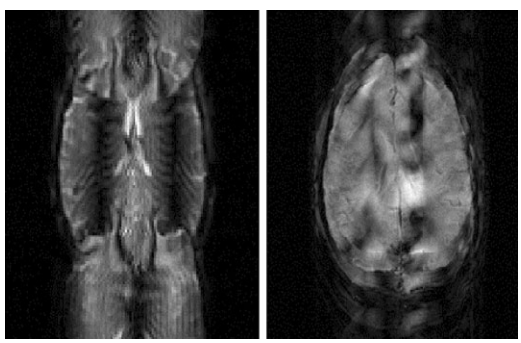

Figure 4. Typical motion artifact: ghosting and large signal variations across the image (image courtesy of F. Hennel).

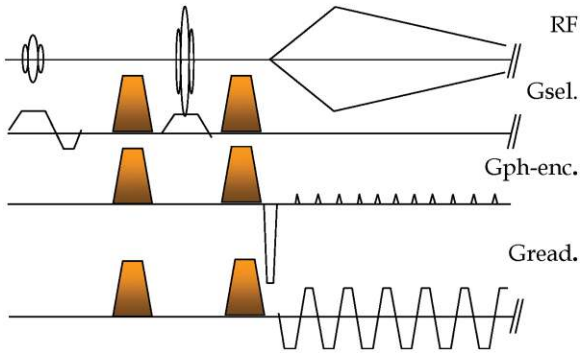

Figure 5. Typical time diagram of a diffusion-sensitized EPI sequence (diffusion gradient pulses are filled patterns). [Color figure can be viewed in the online issue, which is available at www.interscience.wiley.com.]

which are more severe with strong gradient pulses or in the presence of important motion (Fig. 4). Moreover, since the signal is no longer confined to the original voxels but is spread out over the whole image, there is an artifactual signal loss that increases with gradient strength and leads to an overestimation of the ADC. This overestimation is highly variable and can, in principle, be disentangled from the systematic error obtained from eddy-current artifacts.

One way to cure motion artifacts is to synchronize the acquisition with the source of motion, for example using cardiac gating. Then the motion-induced phase shifts will remain identical for each echo, avoiding signal loss or ghosting. Unfortunately, cardiac gating is not always reliable and increases the acquisition times. Another method is to monitor motion using so-called "navigator echoes" (21–23,37–40). The idea behind navigator echoes is to record an additional non-phase-encoded echo that is then used to correct the phase of all other echoes recorded. The effects of both displacement and rotation can only be adequately corrected if the diffusion-sensitizing gradient and the phase-encoding imaging gradient are parallel. If complete freedom in the direction of the diffusion-sensitizing gradient is required, a second navigator echo can be applied perpendicular to the first. Navigator echoes may work well, but they are not easy to manipulate (41).

Ultimately, the only way to avoid motion artifacts is to either eliminate motion (as done in studies with anesthetized animals) or use an MRI sequence that is less prone to motion artifacts. This is typically the case for echo-planar imaging (EPI). With EPI an image is acquired within a single shot, the duration of which is typically around 100 msec, and hence motion is effectively frozen during the acquisition. Diffusion MRI entered the clinical domain when manufacturers made EPI available on their MRI scanners, and EPI is now the gold standard for clinical diffusion MRI (Fig. 5). In addition, parallel imaging can also be used to shorten the echo train, and thus the acquisition time, resulting in a lower sensitivity to motion.

EPI often provides less spatial resolution than conventional sequences due to gradient limitations, and the EPI sequence is sometimes run using two or more shots (multishot EPI). Motion artifacts may then reappear, but echo navigators can be used very successfully to mitigate them. Interestingly, although motion-induced ghosting is totally cured with EPI, motion may still act in a hidden way on the data (ghosting may also still be present, but from other sources (see below)). The images look clean, but problems may arise when the ADC is calculated from a series of differently sensitized images (using a range of b-values). In the presence of motion, a given voxel within the image is not exactly at the same location throughout the data set. For voxels located near the interface between two tissues with different diffusion coefficients, partial volume effects will appear. For each b-factor the content of a particular voxel will shift and result in a signal intensity variation in this voxel. In a plot of log(Signal) vs. b, one obtains a noisier pattern—not a smooth line (or curve). This artifact is mainly seen at the interface between brain and cerebrospinal fluid (CSF), because the ADC of CSF (about 3×10^{-3} m^2/second^{-1}) is more than three times larger than normal brain ADC. The brain ADC is then slightly overestimated and has a larger than expected standard deviation (SD). One cure for this problem is to cardiac-gate the diffusion EPI acquisitions. One may also suppress signal from CSF using dedicated sequences (e.g., inversion-recovery prepared diffusion EPI (42)).

An interesting alternative way to cure motion artifacts is to use a method that does not rely on gradient pulses. Preliminary data have been obtained based on direct diffusion measurements using the distant dipolar field (DDF) method. Diffusion weighting using this effect is unique in that the refocusing "gradient" is carried within the sample, and thus the macroscopic mo-

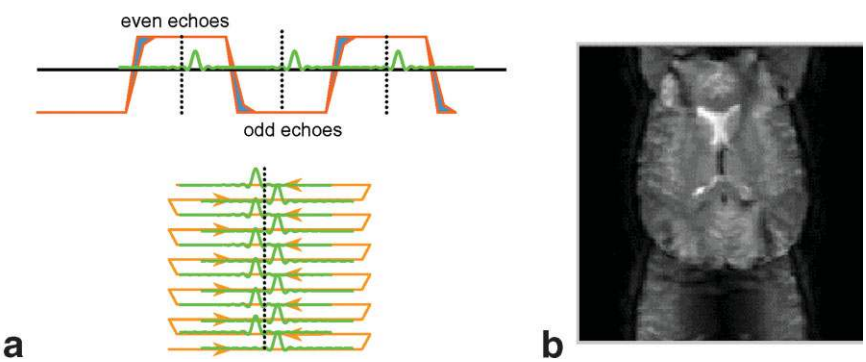

Figure 6. Effects of eddy currents. **a:** Eddy currents modify the actual shape of the gradient pulses. As a result, echo signals are not refocused with a slight delay (top). In k-space, because of the back-and-forth trajectories used between the even and odd lines, the echoes are misaligned. **b:** After reconstruction this misalignment produces a ghost image shifted by half the FOV (N/2 ghost) (image courtesy of F. Hennel). [Color figure can be viewed in the online issue, which is available at www.interscience.wiley.com.]

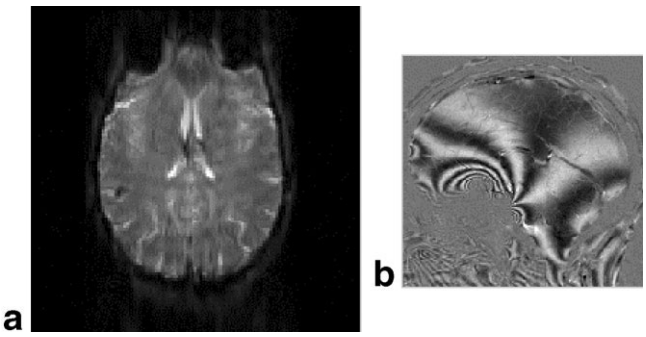

Figure 7. a: Geometric distortion induced by magnetic susceptibility differences among brain tissue (frontal lobe), bone, and air-filled sinuses. **b:** The phase map clearly shows how the B_0 field homogeneity is destroyed near the interfaces. Such phase maps can be used to unwrap distortions.

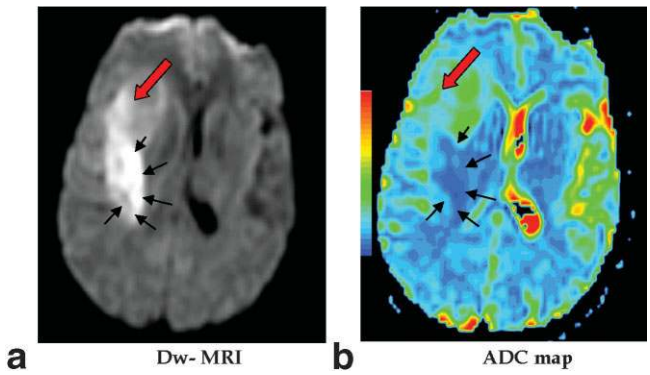

Figure 8. a: The bright signal area (arrows) on the DW image could be interpreted as low diffusion (acute stroke) or increased T2 (older stroke). **b:** The ADC map clearly shows that this area has a low ADC. On the other hand, the adjacent anterior region has a high ADC (red arrow), although the signal on the DW image is slightly elevated (T2 contribution) (image courtesy of C. Oppenheim).

tion of the sample is not expected to interfere with signal formation (43).

EPI ARTIFACTS

It is often the case that the cure for a problem will result in other problems. Unfortunately, this is true for EPI, which is very vulnerable to artifacts. In this section we will look at artifacts that are no longer specific to diffusion MRI, but apply to other methods based on EPI.

EPI spatial resolution is often coarse (around 2 mm) due to hardware limitations. Furthermore, those hardware limitations often result in long echo trains (typically 50–100 msec), which leads to image blurring (also called point-spread function (PSF) artifact), as T2*-related signal decay occurs during the signal readout (which also results from poor shimming). Recently developed parallel acquisition techniques, which allow signals to be collected simultaneously using an array of several radiofrequency (RF) coils, are very promising tools to correct for these limitations (44,45). The two main Achilles' heels of EPI, however, are low bandwidth and eddy currents.

Back to Eddy Currents: Ghosting

We have already seen how the diffusion gradient pulses can generate eddy currents and modify the actual gradient pulse shape. With EPI, unbalanced areas between gradient pulses translate into a magnetization phase shift that is visible as "ghosts" in the reconstructed images. This results from a misalignment of the echoes in k-space created. Because of the back-and-forth trajectory in k-space used in EPI, the phase shifts create a difference of the position of the echo center from line to line in the k-space raw data (Fig. 6). The data appear modulated along the phase-encoding direction with a frequency equal to half the phase-encoding bandwidth. When the data are Fourier transformed, this modulation results in an image duplicated at half the field of view (FOV). This ghosting structure is frequently referred to as an "N/2" ghost (Fig. 6b). The EPI sequence itself is also source of eddy currents because the gradients along the readout direction must be switched very fast with very large intensities.

The first (and mandatory) correction of such image ghosts is to reduce eddy currents at the source by using shielded or "screened" gradient coils, as explained for the diffusion gradient pulses. However, residual eddy current may persist, and there are other sources of phase shifts that may lead to some degree of ghosting. Elimination of the N/2 ghost then requires a critical calibration of the timing between signal digitization and gradient activity. Delays of a few microseconds result in line-by-line phase discrepancies because of the alternating left–right trajectory along the readout axis in k-space. These errors can be tuned out in hardware by adjusting the sampling clock, and may be adjusted further in software by adding an appropriate phase shift to the raw data ("trim"). A very successful approach to ghost correction is to acquire a reference scan in the absence of phase encoding and to use this as a basis for determining the time-dependent phase shifts. This reference scan is often included in the preparation stage (calibrating the frequency, transmitter, and re-

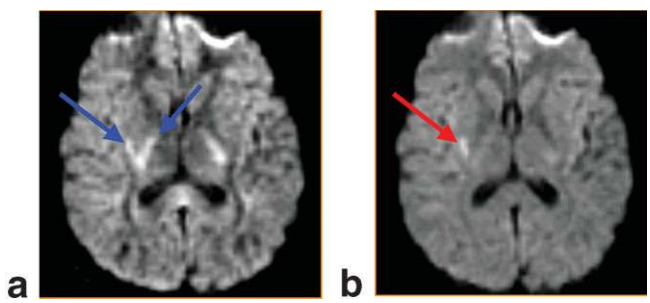

Figure 9. a: The bright signal areas on each side on the third ventricle (blue arrows) on this DW image acquired with diffusion gradients along the x-direction could be interpreted as low diffusion (acute stroke). **b:** The ADC trace-weighted map (right) shows that most of the high signal comes from diffusion anisotropy. Only a small area (red arrow) really corresponds to a decreased ADC and potentially an acute stroke event (image courtesy of C. Oppenheim).

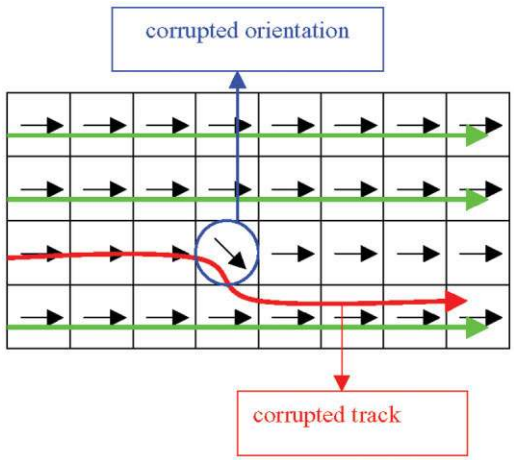

Figure 10. Scheme showing how an error in determining the main direction of diffusivity in a voxel (for instance due to poor SNR or geometric distortion) can result in an erroneous fiber track.

ceiver gain, etc.) performed before each examination. Eddy currents may also cause image distortion (33,46).

Bandwidth Issue

The pixel bandwidth refers to the difference in MR frequencies between adjacent pixels, whereas the image bandwidth refers to the total range of frequencies that make up an image. In conventional imaging, the difference in MR frequencies between adjacent pixels (or bandwidth per pixel) is around 100 Hz at 1.5T. Any source of frequency shift larger than 100 Hz will thus translate to a pixel shift. For instance, the chemical shift between fat and water is about 220 Hz at 1.5T. In this case the fat and water components of a single voxel will be shifted along the readout direction from one another by about 1 or 2 pixels, which is an acceptable imaging artifact. Similarly, magnetic interfaces between bone or air-filled cavities (sinuses) and water-containing tissues generate local gradients and frequency-shift that are generally on the order of the pixel bandwidth and result in similar limited artifacts.

Although the pixel bandwidth in EPI is very high (kHz) due to the rapid sampling rate along the readout axis, the continuous "phase-encoding" scheme used in EPI results in a relatively low bandwidth along the phase-encoding axis (30 Hz/pixel is typical). This causes severe artifacts to occur in EPI in the presence of local frequency shifts. However, artifacts will now occur along the phase-encoding direction.

Chemical-Shift Artifacts

At 1.5T, for example, using a 30-Hz/pixel bandwidth, fat and water are now displaced by about 8 pixels. Furthermore, the voxel sizes in EPI are usually rather large, for the reasons discussed above. Using a more or less typical 3-mm voxel, fat and water may be displaced from one another by 2.5 cm. This problems scales with field strength, so that in a 3T scanner the fat/water chemical shift approaches 5 cm.

Fortunately, in the vast majority of cases, only the water component of the MR signal is of clinical interest. This is always the case in brain diffusion imaging, where the lipid content of the brain is very low and the dominant source of fat signal is the component found in the skull bone and skin. It is therefore reasonable to simply suppress the fat signal. Usually this is done by applying a fat-saturation pulse prior to imaging (90° pulse at the fat frequency). After this pulse the fat signal will be in the transverse plane and it can be dephased easily by applying a gradient pulse. This chemical shift saturation method does require excellent magnetic field homogeneity so that the frequencies of fat and water will be well resolved; however, this is usually not a problem.

Geometric Distortion and Susceptibility Artifacts

EPI requires a very homogeneous magnetic field, and magnetic interfaces result in local image distortion or signal dropout (47). The low bandwidth of EPI in the phase-encoding direction causes a much less manageable artifact in shape distortion. Even in a well-shimmed magnet, the human head will magnetize unevenly and thus the MR frequency may differ from point to point by more than one part per million (ppm) and more than 125 Hz at 3T. These small frequency differences result in spatial displacement of several pixels in the resulting images (Fig. 7). The shape distortions are a frequent cause of concern in neuroimaging, since it is often desirable to superimpose brain images of activation or WM tracts onto higher-resolution structural images that are usually acquired conventionally (e.g., with

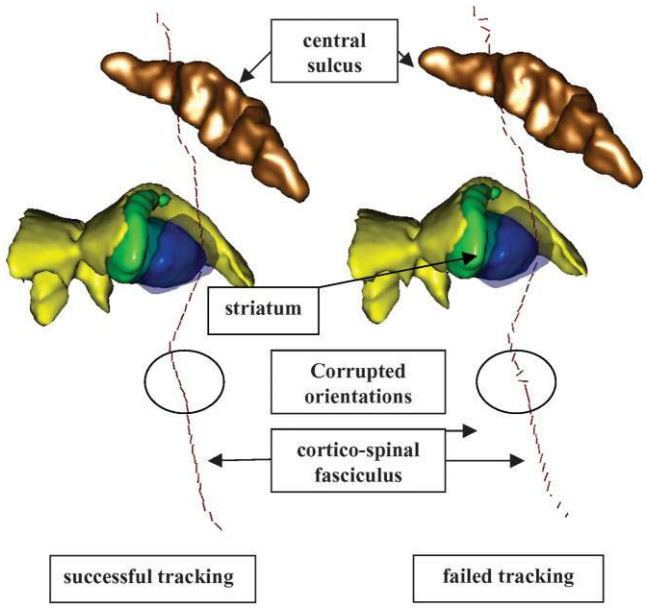

Figure 11. Impact of the presence of corrupted orientations on the track calculation. On the left, a corticospinal fasciculus, starting from the primary motor area in the central sulcus, going through the internal capsule toward the brain stem, was calculated using a regularization approach. On the right, some voxels with corrupted eigenvectors led to a failure of the algorithm (track interruption).

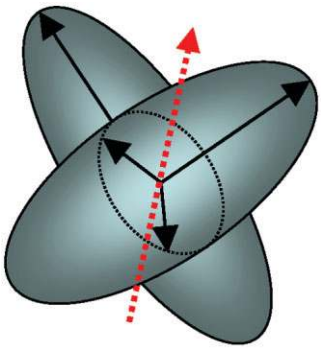

Figure 12. Limitation of the DTI model in heterogeneous voxels. Two fiber bundles are crossing inside a voxel at 90° leading to the direction of highest diffusivity (red arrow) that does not fit with any of the actual bundle directions.

a much higher bandwidth). In this case the diffusion maps will not be registered properly with the structural data set.

Generally, however, this artifact is correctable. It is possible to measure the magnetic field in the head using a dedicated gradient-echo MR sequence and then apply a correction to the MR image to shift the signal to its correct location (48). Other approaches aim at correcting field heterogeneities in situ (49). Parallel imaging can also be used to minimize geometric distortion by reducing the echo train length (50) and thus the overall amount of phase shift. This method is particularly efficient for blood oxygen level-dependent (BOLD) fMRI, where EPI can be used with short TEs. In diffusion EPI the gain is less obvious because longer TEs are imposed to accommodate the diffusion-encoding gradient pulses. However, shorter echo trains allow for a more efficient use of time and slightly reduced TEs, which in turn improves the SNR. This advantage could become critical in diffusion EPI, especially at high b-values.

DIFFUSION MRI PROCESSING AND INTERPRETATION PITFALLS

In this section we will briefly touch upon caveats regarding diffusion MRI that relate more to the limitations of the method rather than to artifacts resulting from the MRI scanner.

First, let us keep in mind that diffusion MRI is successful primarily in the brain. Outside the brain, motion and susceptibility artifacts become much more severe. Another problem is that since body tissues usually have shorter T2s, shorter TEs must be used, which in turn limits the range of b-values that can be reached. Lower b-values and shorter T2s always lead to poor SNR issues. Susceptibility artifacts and the requirement for short TEs sometimes also preclude the use of EPI. Alternative motion-robust, imaging schemes, such as line-scan, slab-scan (51,52), and periodically rotated overlapping parallel lines with enhanced reconstruction (PROPELLER) (53), may then become handy. Recent outstanding results in the application of diffusion MRI in the body to detect cancer and metastases (as an alternative to FDG-PET) were achieved through the use of parallel imaging and phased-array coils (54).

A common pitfall in brain diffusion MRI is known as the "T2-shine-through" artifact. Since "diffusion-weighted" (DW) images are actually T2-weighted images that have been made sensitive to diffusion by the use of strong gradient pulses, the image contrast, of course, results from diffusion *and* T2. A region with a "bright" signal may thus come from a reduced ADC or an increased T2. This issue may become serious in stroke cases, since a reduced ADC means a very recent infarct, while an increased T2 is usually associated with a older infarct. One can easily eliminate this problem by calculating an ADC image in which the contrast depends only on diffusion (Fig. 8).

Another common artifact comes from anisotropic diffusion. If diffusion sensitization is obtained only along one direction, anisotropic diffusion tissues (such as WM) oriented perpendicularly to this direction will show reduced diffusion and appear bright on the DW image, potentially mimicking a recent infarct. There is also an easy solution for this: images can be acquired along several directions. Ideally, a whole DT acquisition would be obtained. An image of the trace of the DT would average out any directional effect and remove the

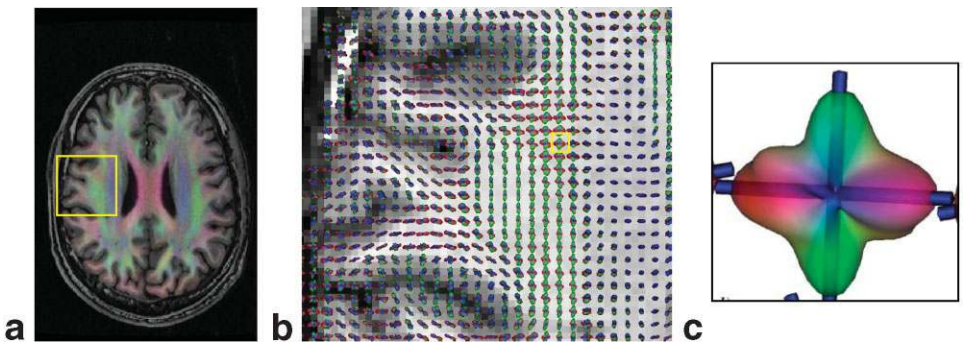

Figure 13. Example of Q-ball HARDI data. **a:** Color-coded orientation map superimposed onto a standard T1 anatomy. **b:** This zoomed-in window of the yellow square in image a displays Q-ball models estimated at each voxel from an acquisition containing 500 diffusion orientations at b = 3000 seconds/mm^2. **c:** One voxel has been isolated (yellow square in b) and zoomed-in to display the four lobes corresponding to a fiber crossing.

artifact (Fig. 9). Trace-weighted scans may also be acquired directly (55).

It should be noted for the sake of completeness that there are other pitfalls, such as the effects of local gradients caused by magnetic susceptibility induced by tissue interfaces or even local high doses of contrast agent, that may lead to miscalculation of ADCs.

DTI WM FIBER-TRACKING PITFALLS

Other pitfalls are specific to the DTI method, due either to biases in the calculation of the DT components or to limitations in the tracking algorithm.

By processing DTI data in each voxel, one can define three main directions of diffusion at each brain location (see Ref. 56 for a review). Assuming that the direction associated with the highest diffusivity corresponds to the underlying orientation of the tissue, one can easily build two-dimensional maps of this orientation over the brain (e.g., by defining a color code for three-dimensional space (7,57)). Such maps are a convenient way to display a compact representation of well known cerebral WM fiber bundles, such as the corpus callosum and the pyramidal tracts, but they cannot render the three-dimensional trajectory of these fiber bundles well.

Reconstruction of fiber bundle trajectories from DTI data assumes that from a given voxel in the brain, a pathway or fiber tract can be defined, looking forward and backward along the direction of maximum diffusion (i.e., the principal eigenvector in the case of DTI) (58,59). Even though it is the most widely used method, this approach strongly depends on the quality of the estimated principal diffusion direction (the so-called eigenvector). It fails as soon as an eigenvector is corrupted by acquisition noise, as depicted in Figs. 10 and 11. More generally, fiber tracking belongs to the category of ill-posed problems and cannot efficiently be solved with "blind" algorithms that only consider the fiber under construction and forget the remaining fibers. Several alternative methods have been introduced to correct for corrupted orientations on a global level; some rely on a Markovian description of the orientation field (36), while others use front propagation algorithms (60) or random walk schemes (61) in which robustness is achieved by means of statistics.

However, a more important shortcoming of DTI is that whatever the robustness of the tracking algorithm used, the model cannot deal correctly with voxels that contain several populations of fibers that are not necessarily characterized by the same orientation, and may be crossing. Unfortunately, the DT model assumes a homogeneous population inside the voxel (free, Gaussian diffusion) and fails at describing more realistic, heterogeneous populations. For instance, the case of two bundles crossing at 90° yields an oblate tensor ellipsoid (Fig. 12). The principal eigenvector of such a voxel does not have a clear relation to the underlying structure orientation, and may be the source of abrupt (non-anatomical) interruptions of fiber tracts inside WM or erroneous connections between adjacent fibers.

Several models have been introduced to overcome the limitations of DTI. In the high-angular-resolution diffusion imaging (HARDI) class of models, a local orientation distribution function (ODF), which may exhibit several lobes corresponding to different populations, is processed for each voxel. These models include Q-space imaging (QSI) (62) and inherited diffusion spectrum imaging (DSI) (63) or Q-ball imaging (QBI) (64), generalized DTI (gDTI) (65), spherical deconvolution model (66), maximum entropy models, and persistent angular structure MRI (PASMRI) (67). All HARDI techniques aim to bypass the free (Gaussian) diffusion assumption made during the diffusion process, but at the expense of a huge amount of data required for the model to be robust, and consequently of longer acquisition times. These models are quite efficient for managing fiber crossings (Fig. 13), but they are still unable to describe merging, splitting, or bending fibers. However, using HARDI models locally along with robust tracking algorithms that can deal with crossing/merging/splitting patterns greatly improves results.

Another issue with tracking algorithms is the need to limit the region of interest (ROI) where fiber bundles are tracked, and consequently to define a robust stop criterion. One common way to do this is to extract a binary mask of the WM from a gray matter (GM)/WM segmentation using a standard T1-weighted MR image. However, this requires a perfect match between diffusion and T1 images, which is not so easy to obtain due to the residual distortions present in diffusion EPI data, as explained above. An alternative solution is to stop the algorithm as soon as the anisotropy value falls under an empirically determined value; however, the results then become operator-dependent. Furthermore, although anisotropy may be small in voxels that contain merging or splitting fibers, the tracking process should not be stopped at such locations (68).

In conclusion, diffusion MRI has become established as a mature technique with great potential for health care and neurosciences. Considerable progress has been made since the initial studies were performed more than 20 years ago, especially in overcoming hardware limitations and methodological shortcomings. As a result, diffusion MRI has been installed on several thousands of clinical MRI scanners worldwide, and today very accurate diffusion measurements can be made in patients. Beautiful images of brain connectivity often make the cover of prestigious journals. Still, we must remain aware that diffusion MRI still suffers from some pitfalls and artifacts that are not always easy to detect or cure. Active research is currently under way to further expand the limits and the potential of diffusion MRI, in particular to elucidate the diffusion process in biological tissues. With such knowledge, diffusion MRI is likely to emerge as a key approach for exploring brain function at the neuronal level (69), and as a molecular imaging tool for detecting cancer (54).

REFERENCES

1. Einstein A. (Collection of papers translated from the German). In: Furthe R, Cowper AD, editors. Investigations on the theory of Brownian motion. New York: Dover; 1956.
2. Le Bihan D. Looking into the functional architecture of the brain with diffusion MRI. Nat Rev Neurosci 2003;4:469–480.

3. Le Bihan D, Breton E, Lallemand D, Grenier P, Cabanis E, Laval Jeantet M. MR Imaging of intravoxel incoherent motions: application to diffusion and perfusion in neurologic disorders. Radiology 1986;161:401–407.
4. Moseley ME, Kucharczyk J, Mintorovitch J, et al. Diffusion-weighted MR imaging of acute stroke: correlation with T2-weighted and magnetic susceptibility-enhanced MR imaging in cats. AJNR Am J Neuroradiol 1990;11:423–429.
5. Warach S, Chien D, Li W, Ronthal M, Edelman RR. Fast magnetic resonance diffusion-weighted imaging of acute human stroke. Neurology 1992;42:1717–1723.
6. Moseley ME, Cohen Y, Kucharczyk J. Diffusion-weighted MR imaging of anisotropic water diffusion in cat central nervous system. Radiology 1990;176:439–446.
7. Douek P, Turner R, Pekar J, Patronas NJ, Le Bihan D. MR color mapping of myelin fiber orientation. J Comput Assist Tomogr 1991; 15:923–929.
8. Basser PJ, Mattiello J, Le Bihan D. Estimation of the effective self-diffusion tensor from the NMR spin echo. J Magn Reson 1994; 103:247–254.
9. Basser PJ, Mattiello J, Le Bihan D. MR diffusion tensor spectroscopy and imaging. Biophys J 1994;66:259–267.
10. Hermoye L, Saint-Martin C, Cosnard G, et al. Pediatric diffusion tensor imaging: normal database and observation of the white matter maturation in early childhood. Neuroimage 2006;29:493–504.
11. Neil J, Miller J, Mukherjee P, Huppi PS. Diffusion tensor imaging of normal and injured developing human brain—a technical review. NMR Biomed 2002;15:543–552.
12. Le Bihan D, Breton E. Imagerie de diffusion in vivo par résonance magnétique nucléaire. CR Acad Sci Paris 1985;301:1109–1112.
13. Merboldt KD, Hanicke W, Frahm J. Self-diffusion NMR imaging using stimulated echoes. J Magn Reson 1985;64:479–486.
14. Taylor DG, Bushell MC. The spatial mapping of translational diffusion coefficients by the NMR imaging technique. Phys Med Biol 1985;30:345–349.
15. Le Bihan D. Molecular diffusion, tissue microdynamics and microstructure. NMR Biomed 1995;8:375–386.
16. Stejskal EO, Tanner JE. Spin diffusion measurements: spin echoes in the presence of a time-dependent field gradient. J Chem Phys 1965;42:288–292.
17. Le Bihan D. In: Le Bihan D, editor. Diffusion and perfusion magnetic resonance imaging. Applications to functional MRI. New York: Raven Press; 1995.
18. Tanner JE. Self diffusion of water in frog muscle. Biophys J 1979; 28:107–116.
19. Tanner JE. Transient diffusion in a system partitioned by permeable barriers. Application to NMR measurements with a pulsed field gradient. J Chem Phys 1978;69:1748–1754.
20. Cooper RL, Chang DB, Young AC, Martin J, Ancker-Johnson B. Restricted diffusion in biophysical systems. Biophys J 1974;14: 161–177.
21. Vavrek RM, MacFall JR. Hardware considerations for diffusion/perfusion imaging. In: Le Bihan D, editor. Diffusion and perfusion magnetic resonance imaging. Applications to functional MRI. New York: Raven Press; 1995. p 67–72.
22. Tanner JE. Use of the stimulated-echo in NMR diffusion studies. J Chem Phys 1970;52:2523–2526.
23. Reese TG, Heid O, Weisskoff RM, Wedeen VJ. Reduction of eddy-current-induced distortion in diffusion MRI using a twice-refocused spin echo. Magn Reson Med 2003;49:177–182.
24. Bammer R, Markl M, Barnett A, et al. Analysis and generalized correction of the effect of spatial gradient field distortions in diffusion-weighted imaging. Magn Reson Med 2003;50:560–9.
25. Tofts PS, Lloyd D, Clark CA, et al. Test liquids for quantitative MRI measurements of self-diffusion coefficient in vivo. Magn Reson Med 43:368–74.
26. Neeman M, Freyer JP, Sillerud LO. Pulse-gradient spin-echo studies in NMR imaging. Effects of the imaging gradients on the determination of diffusion coefficients. J Magn Reson 1990;90: 303–312.
27. Mattiello J, Basser PJ, Le Bihan D. The b-matrix in diffusion tensor echo-planar imaging. Magn Reson Med 1997;37:292–300.
28. Mansfield P, Chapman BE. Active magnetic screening of gradient coils in NMR imaging. J Magn Reson 1986;66:573–576.
29. Papadakis NG, Martin KM, Pickard JD, Hall LD, Carpenter TA, Huang CLH. Gradient preemphasis calibration in diffusion-weighted echo-planar imaging. Magn Reson Med 2000;44:616–624.
30. Schmithorst VJ, Dardzinski BJ. Automatic gradient preemphasis adjustment: a 15-minute journey to improved diffusion-weighted echo-planar imaging. Magn Reson Med 2002;47:208–212.
31. Terpstra M, Andersen PM, Gruetter R. Localized eddy current compensation using quantitative field mapping. J Magn Reson 1998; 131:139–143.
32. Haselgrove JC, Moore JR. Correction for distortion of echo-planar images used to calculate the apparent diffusion coefficient. Magn Reson Med 1996;36:960–964.
33. Jezzard P, Barnett AS, Pierpaoli C. Characterization of and correction for eddy current artifacts in echo planar diffusion imaging. Magn Reson Med 1998;39:801–812.
34. Calamante F, Porter DA, Gadian DG, Connelly A. Correction for eddy currents induced B_0 shifts in diffusion-weighted echo-planar imaging. Magn Reson Med 1999;41:95–102.
35. Rohde GK, Barnett AS, Basser PJ, Marenco S, Pierpaoli C. Comprehensive approach for correction of motion and distortion in diffusion-weighted MRI. Magn Reson Med 2004;51:103–114.
36. Poupon C, Clark CA, Frouin V, et al. Regularization of diffusion-based direction maps for the tracking of brain white matter fascicles. Neuroimage 2000;195.12:184–195.
37. Ordidge RJ, Helpern JA, Qing ZX, Knight A, Nagesh V. Correction of motional artifacts in diffusion-weighted MR images using navigator echoes. Magn Reson Imaging 1994;12:455–460.
38. Anderson AW, Gore JC. Analysis and correction of motion arifacts in diffusion weighted imaging. Magn Reson Med 1994;32:379–387.
39. De Crespigny AJ, Marks MP, Enzmann DR, Moseley ME. Navigated diffusion imaging of normal and ischemic human brain. Magn Reson Med 1995;30:720–728.
40. Marks MP, De Crespigny A, Lentz D, Enzmann D, Albers GW, Moseley ME. Acute and chronic stroke: navigated spin-echo diffusion-weighted MR imaging. Radiology 1996;199:403–408.
41. Miller KL, Pauly JM. Nonlinear phase correction for navigated diffusion imaging. Magn Reson Med 2003;50:343–353.
42. Andersson L, Bolling M, Wirestam R, Holtas S, Stahlberg F. Combined diffusion weighting and CSF suppression in functional MRI. NMR Biomed 2002;15:235–240.
43. Kennedy SD, Zhong JH. Diffusion measurements free of motion artifacts using intermolecular dipole-dipole interactions. Magn Reson Med 2004;52:1–6.
44. Bammer R, Auer M, Keeling SL, et al. Diffusion tensor imaging using single-shot SENSE-EPI. Magn Reson Med 2002;48:128–136.
45. Bammer R, Keeling SL, Augustin M, et al. Improved diffusion-weighted single-shot echo-planar imaging (EPI) in stroke using sensitivity encoding (SENSE). Magn Reson Med 2001;46:548–554.
46. Shen YJ, Larkman DJ, Counsell S, Pu IM, Edwards D, Hajnal JV. Correction of high-order eddy current induced geometric distortion in diffusion-weighted echo-planar images. Magn Reson Med 2004; 52:1184–1189.
47. Basser PJ, Jones DK. Diffusion-tensor MRI: theory, experimental design and data analysis—a technical review. NMR Biomed 2002; 15:456–467.
48. Jezzard P, Balaban RS. Correction of geometric distortion in echo-planar imaging from B_0 field variations. Magn Reson Med 1995;34: 65–73.
49. Gu H, Feng HH, Zhan W, et al. Single-shot interleaved Z-shim EPI with optimized compensation for signal losses due to susceptibility-induced field inhomogeneity at 3 T. Neuroimage 2002;17:1358–1364.
50. Jaermann T, Pruessmann KP, Valanis A, Kollias S, Boesiger P. Influence of SENSE on image properties in high-resolution single-shot echo-planar DTI. Magn Reson Med 2006;55:335–342.
51. Maier SE, Gudbjartsson H, Patz S, et al. Line scan diffusion imaging: characterization in healthy subjects and stroke patients. AJR Am J Roentgenol 1998;171:85–93.
52. Maier SE. Slab scan diffusion imaging. Magn Reson Med 2001;46: 1136–1143.
53. Pipe JG. Motion correction with PROPELLER MRI: application to head motion and free-breathing cardiac imaging. Magn Reson Med 1999;42:963–969.

54. Takahara T, Imai Y, Yamashita T, Yasuda S, Nasu S, van Cauteren M. Diffusion-weighted whole-body imaging with background body signal suppression (DWIBS): technical improvement using free breathing, STIR and high-resolution 3D display. Radiation Med 2004;22:275–282.
55. Mori S, Van Zijl PCM. Diffusion weighting by the trace of the diffusion tensor within a single scan. Magn Reson Med 1995;33: 41–52.
56. Le Bihan D, Mangin JF, Poupon C, Clark CA, Pappata S, Molko N. Diffusion tensor imaging: concepts and applications. J Magn Reson Imaging 2001;13:534–546.
57. Pajevic S, Pierpaoli C. Color schemes to represent the orientation of anisotropic tissues from diffusion tensor data: application to white matter fiber tract mapping in the human brain. Magn Reson Med 1999;42:526–540.
58. Jones DK, Simmons A, Williams SC, Horsfield MA. Non-invasive assessment of axonal fiber connectivity in the human brain via diffusion tensor MRI. Magn Reson Med 2000;42:37–41.
59. Mori S, van Zijl PCM. Fiber tracking: principles and strategies—a technical review. NMR Biomed 2002;15:468–480.
60. Parker GJ, Alexander DC. Probabilistic Monte Carlo based mapping of cerebral connections utilizing whole-brain crossing fiber information. Info Process Med Imaging 2003;18:684–695.
61. Perrin M, Poupon C, Rieul B, et al. Validation of q-ball imaging with a diffusion fiber-crossing phantom on a clinical scanner. Phil Trans R Soc Lond (Biol) 2005;360:881–891.
62. Assaf Y, Cohen Y. Structural information in neuronal tissue as revealed by q-space diffusion NMR spectroscopy of metabolites in bovine optic nerve. NMR Biomed 1999;12:335–344.
63. Wedeen VJ, Hagm, Tseng WY, Reese TG. Mapping complex tissue architecture with diffusion spectrum magnetic resonance imaging. Magn Reson Med 2005;54:1377–1386.
64. Tuch DS. Q-ball imaging. Magn Reson Med 2004;53:1358–1372.
65. Liu CL, Bammer R, Acar B, Moseley ME. Characterizing non-Gaussian diffusion by using generalized diffusion tensors. Magn Reson Med 2004;51:924–937.
66. Tournier JD, Calamante F, Gadian DG, Connelly A. Direct estimation of the fiber orientation density function from diffusion-weighted MRI data using spherical deconvolution. Neuroimage 2004;23:1176–1185.
67. Alexander DC. Multiple-fiber reconstruction algorithms for diffusion MRI. Ann NY Acad Sci 2005;1064:113–133.
68. Jones DK, Basser PJ. "Squashing peanuts and smashing pumpkins": how noise distorts diffusion-weighted MR data. Magn Reson Med 2004;52:979–993.
69. Darquie A, Poline JB, Poupon C, Saint-Jalmes H, Le Bihan D. Transient decrease in water diffusion observed in human occipital cortex during visual stimulation. Proc Natl Acad Sci USA 2001;98:9391–9395.